Unusual Pressure-Induced Periodic Lattice Distortion in SnSe$_2$

Jianjun Ying,[1,2] Hari Paudyal,[3] Christoph Heil,[4,5] Xiao-Jia Chen,[6] Viktor V. Struzhkin,[1] and Elena R. Margine[3,*]

[1]*Geophysical Laboratory, Carnegie Institution of Washington, Washington, DC 20015, USA*
[2]*HPCAT, Geophysical Laboratory, Carnegie Institution of Washington, Argonne, Illinois 60439, USA*
[3]*Department of Physics, Applied Physics, and Astronomy, Binghamton University-SUNY, Binghamton, New York 13902, USA*
[4]*Department of Materials, University of Oxford, Parks Road, Oxford OX1 3PH, United Kingdom*
[5]*Institute of Theoretical and Computational Physics, Graz University of Technology, NAWI Graz, 8010 Graz, Austria*
[6]*Center for High Pressure Science and Technology Advanced Research, Shanghai 201203, China*

We performed high-pressure x-ray diffraction (XRD), Raman, and transport measurements combined with first-principles calculations to investigate the behavior of tin diselenide (SnSe$_2$) under compression. The obtained single-crystal XRD data indicate the formation of a $(1/3, 1/3, 0)$-type superlattice above 17 GPa. According to our density functional theory results, the pressure-induced transition to the commensurate periodic lattice distortion (PLD) phase is due to the combined effect of strong Fermi surface nesting and electron-phonon coupling at a momentum wave vector $\mathbf{q} = (1/3, 1/3, 0)$. In contrast, similar PLD transitions associated with charge density wave (CDW) orderings in transition metal dichalcogenides (TMDs) do not involve significant Fermi surface nesting. The discovered pressure-induced PLD is quite remarkable, as pressure usually suppresses CDW phases in related materials. Our findings, therefore, provide new playgrounds to study the intricate mechanisms governing the emergence of PLD in TMD-related materials.

Transition metal dichalcogenides (TMDs) and similar layered materials have attracted significant attention in recent years due to their novel electronic and optical properties [1,2]. Bulk TMDs exhibit rich physics and have a promising potential for technological applications [3,4]. Coexisting charge density wave (CDW) order and superconductivity were often found at low temperatures in metallic TMDs, providing an ideal platform to investigate the interplay of these quantum phases [3,5]. Various commensurate modulated superstructures related to the CDW have been observed in TMDs, such as a $\sqrt{13} \times \sqrt{13} \times 1$ superlattice in $1T$-TaX_2($X =$ S, Se), a $3 \times 3 \times 1$ in $2H$-MSe$_2$ ($M =$ Nb, Ta) and a $2 \times 2 \times 2$ superlattice in $1T$-TiSe$_2$ [6–8], and their origins have been to a large part attributed to strong electron-phonon coupling (EPC) for particular phonon modes and wave vectors [9–11]. Many novel physical properties were recently discovered in TMDs: large positive magnetoresistance was observed at low temperatures in WTe$_2$ [12], and both WTe$_2$ and MoTe$_2$ were suggested as type II Weyl semimetal candidate materials [13,14]. Insulator-metal transitions and superconductivity were also observed in compressed TMDs [4,15–18], raising expectations of novel phenomena in related new materials under high-pressure conditions.

Similar to related TMDs, SnSe$_2$ is a semiconductor with a bulk band gap of about 1.0 eV [19], and few-layer sheets of SnSe$_2$ were suggested to have potential applications in electronic and optoelectronic devices [20]. It has been proposed that SnSe$_2$ can rapidly and reversibly switch from amorphous to crystalline under laser heating, which leads to significant changes in the optical reflectivity; and thus, provides excellent perspective for data storage applications [21]. Recent theoretical calculations suggested that SnSe$_2$ is unstable above 20 GPa, and that it would probably decompose into Sn$_3$Se$_4$ and Se at high pressures [22,23]. However, there is no experimental confirmation of the proposed decomposition scenario in compressed SnSe$_2$. In this study, we find that SnSe$_2$ can, in fact, be stabilized above ~17 GPa by a periodic lattice distortion (PLD) rather than undergoing a decomposition. This PLD is similar to the CDW order observed in TMDs; however, their origins are quite different, as will be discussed in this Letter.

We performed high-pressure single crystal diffraction measurements on the hexagonal SnSe$_2$ structure ($H1$ phase) (see Supplemental Material [24]). The low-pressure x-ray diffraction (XRD) patterns are consistent with the previously reported data at ambient pressure [39]. When the pressure is increased above 17 GPa, diffraction patterns reveal superlattice reflections at $(1/3, 1/3, 0)$, as shown in Fig. 1. This clearly indicates a tripled unit cell above 17 GPa ($H2$ phase), and the XRD patterns at high pressure can be indexed very well using the $\sqrt{3} \times \sqrt{3} \times 1$ superlattice (Supplemental Fig. S1 [24]). The pressure dependence of the lattice parameters a and c is shown in Fig. 1(c). As is evident from the figure, the normalized in-plane lattice parameter does not show any anomaly across the phase transition. However, the lattice parameter c and, consequently, the volume per formula unit both have a kink around the phase transition.
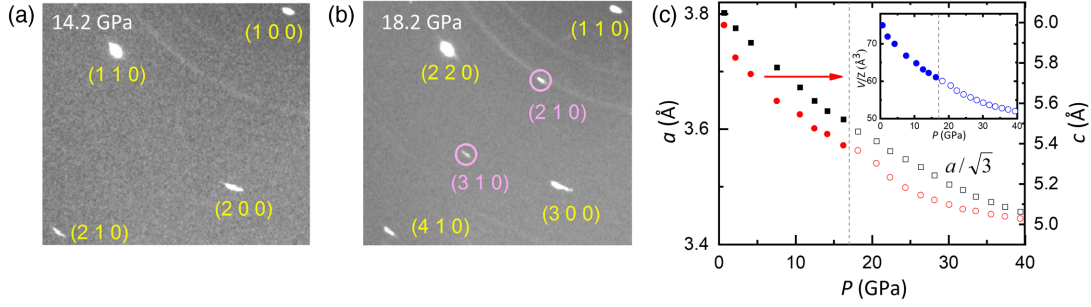
FIG. 1. XRD patterns below (a) and above (b) the phase transition. The sudden appearance of superlattice peaks [magenta circles in (b)] is indicative for a $\sqrt{3} \times \sqrt{3} \times 1$ superlattice formation. (c) The pressure dependence of the lattice parameters a (black squares, left axis) and c (red circles, right axis). The inset shows the pressure dependence of the volume per one formula unit (V/Z). For comparison with the $H1$ phase, a in the $H2$ phase was rescaled by $1/\sqrt{3}$. Small kinks are observed in c and V/Z at 17 GPa.

Taken together, these experimental findings show that the phase transition does not involve a change in the hexagonal lattice structure, but a modulation of the atomic positions as observed in many CDW phases.

In order to elucidate the observed phase transition, we performed first-principles dynamical stability calculations [24]. Based on the phase transformation revealed in the XRD pattern, we began by examining the phonon modes at the Γ point in the $\sqrt{3} \times \sqrt{3} \times 1$ $H1$ superlattice. As the transition pressure is approached, we observe that the two lowest-energy phonon modes soften and exhibit imaginary frequencies above 18 GPa [40]. This is indicative of a lattice instability and in line with findings in metallic TMDs exhibiting a CDW phase [10,11,44,45]. Furthermore, as shown in Fig. 2(a), the decrease in frequency is nonlinear with pressure, reflecting the strong changes in the electronic band structure that take place at the Fermi level (more details later in the manuscript). The squared frequency, on the other hand, exhibits a linear dependence with pressure in the transition region, a characteristic of a soft-mode phase transition described by Landau theory [46]. Incidentally, calculations of the phonon dispersion at 30 GPa in the three-atom $H1$ unit cell show that the lowest-energy vibrational mode has an imaginary frequency at the K point in the

Brillouin zone (BZ), consistent with the BZ folding of the K point of the $1 \times 1 \times 1$ unit cell onto the Γ point of the $\sqrt{3} \times \sqrt{3} \times 1$ supercell (Supplemental Fig. S2 [24]).

We further explored the full potential energy surface of the $H1$ $\sqrt{3} \times \sqrt{3} \times 1$ supercell for the soft phonon modes at 30 GPa. The atoms were displaced according to (i) the eigenvector of the A_{2g} phonon ($H2$-1 phase), (ii) the eigenvector of the A_{2u} phonon ($H2$-2 phase), and (iii) the combined displacements of the two phonon eigenvectors ($H2$-3 phases) [47]. The energy surface has a Mexican hat shape with many local minima within 1 meV/atom from each other (Supplemental Fig. S4(a) [24]). To find the equilibrium configuration for the distorted system, we picked six low-energy points on this surface, for which we performed full geometrical optimization. All selected configurations gain in enthalpy with respect to the $H1$ phase, and become virtually degenerate in enthalpy after relaxation (Supplemental Fig. S4(b) [24]) [48], yet belong to three different space groups [49] (Supplemental Table S1 and Fig. S5 [24]). Noticeably, the out-of-plane modulation in $H2$-3 is an intermediate state along the pathway that transforms $H2$-1 into $H2$-2. We will therefore, without loss of generality, concentrate further only on the $H2$-1 and $H2$-2 phases.

Comparing the enthalpies for the $H1$ and $H2$ structures as function of pressure reveals that the latter are energetically more favorable above 18 GPa, as shown in Fig. 2(b), in very good agreement with our experiments and phonon calculations. Further in depth analysis of the $H2$ derivatives confirmed that they remain degenerate in enthalpy within the 0–40 GPa range considered, and the differences in their vibrational and electronic properties are negligible (Supplemental Figs. S2(c)–S2(d), S6, and S7 [24]).

While our work demonstrates the stabilization of $H1$ derivatives obtained through atomic distortion, previous studies have pointed out the possibility of stable phases obtained through interlayer shifts. Namely, an alternative long-period stacking sequence with space group $R\bar{3}m$ [52] has been recently predicted to be 3.5 meV/atom higher in enthalpy at 0 GPa, but to stabilize with respect to $H1$
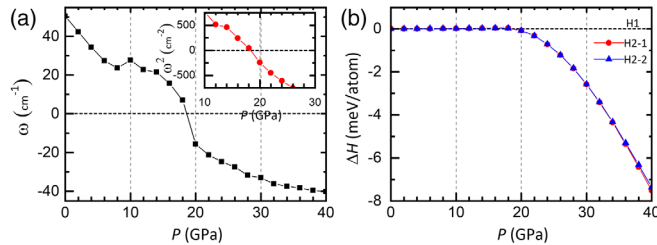

FIG. 2. (a) Calculated softening of the lowest-energy (degenerate) phonon modes, where imaginary phonon frequencies are shown as negative, illustrating the pressure-induced destabilization of the $H1$ phase. The inset shows the squared frequency of the modes. (b) Differences in enthalpies for the considered structures as function of pressure, where the $H1$ phase was chosen as reference.

at 5 GPa [22]. Observation of such polymorphs in high-pressure experiments is not straightforward, as the kinetics of the transformation is likely defined by high-energy barriers of interlayer shifts. Our calculations with finer convergence settings, however, indicate that compared to $H1$, the $R\bar{3}m$ polymorph is virtually degenerate in enthalpy at 0 GPa, reaches a minimum relative enthalpy of ~ 2.3 meV/atom at 6 GPa, and eventually destabilizes by ~ 5.7 meV/atom at 25 GPa. We attribute this behavior to the fact that the application of pressure drastically changes the inter-layer distance, promoting the formation of covalent bonds between Se atoms in adjacent layers (Supplemental Fig. S5 [24]). Such changes in bonding promote a change in compressibility along the c axis, as observed in both experimental and theoretical data (Supplemental Figs. S8 and S9 [24]).

High-pressure transport measurements were performed on $SnSe_2$ single crystals. At low pressures, the resistivity shows a semiconducting behavior, consistent with $SnSe_2$ being a narrow band semiconductor at 0 GPa (Supplemental Fig. S10 [24]). The resistivity decreases under pressure and the temperature dependence becomes flat around 8 GPa, signaling the closure of the band gap. The semiconductor-to-metal transition occurs in the 8–13 GPa range, and a typical metallic behavior with much larger residual-resistance ratio is observed above 17 GPa. Similarly to the room temperature resistivity, the Hall coefficient decreases gradually with increasing pressure and displays a kink at ~ 15 GPa, around the $H1$-to-$H2$ phase transition [53]. These complementary results provide evidence for the Fermi surface (FS) reconstruction across the phase transition.

To investigate the metallization from the theoretical side, we carried out band structure calculations at various pressures. As illustrated in Supplemental Fig. S11 [24], the top of the valence band of $H1$ structure at 0 GPa consists of states with Se p_z and p_{xy} character. The conduction band minimum is formed by Se p_z and p_{xy} orbitals, which hybridize strongly with Sn s orbitals [54]. With increasing pressure, the conduction Se p_{xy} band shifts down and touches the valence Se p_z band at 5–6 GPa, closing the band gap. This pressure-induced metallization is consistent with our resistivity measurements, although the predicted semiconductor-to-metal transition pressure is smaller than the experimental value. This difference is partially due to the underestimation of the band gap in the semilocal density functional theory approximation used in this study [19,55,56]. Band structure calculations employing screened hybrid functional indeed predict a semiconductor-to-metal transition at about 8 GPa [23], in better agreement with experiments. An additional source for the offset could arise from the discrepancy between the calculated and experimental lattice constants in the 5–20 GPa range. Since NaCl provides a slightly non hydrostatic pressure environment [24], we computed the band structure of $H1$ phase by compressing the c axis, as done experimentally. As in
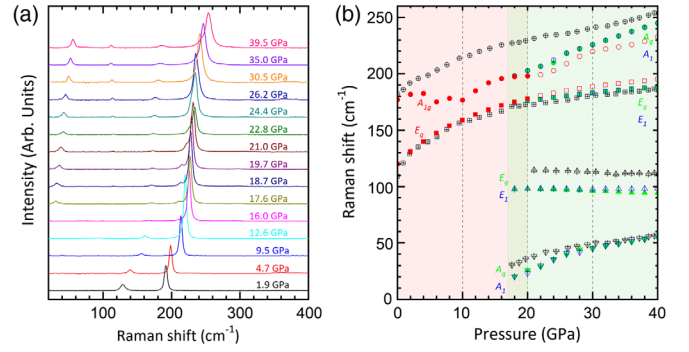

FIG. 3. (a) Selected Raman spectra for various pressures. New modes appear above 17 GPa, indicating the $H1$-to-$H2$ phase transition. (b) Calculated and measured frequency dependence of the Raman-active modes as a function of pressure. The theoretical results are shown as red symbols ($H1$), green symbols ($H2$-1), and blue symbols ($H2$-2). For $H1$, the data before and after the phase transition are shown as filled and open symbols, respectively. The experimental data are shown as black symbols.

$2H$-$MoTe_2$ [57], the out-of-plane compression favors the semiconductor-to-metal transition at a lower pressure; nevertheless, the effect is small (Supplemental Fig. S12 [24]), and the deviation from hydrostatic pressure should have a minor effect on the semiconductor-to-metal transition pressure.

To shed more light on the pressure-induced structural modulations, we performed high-pressure Raman measurements, as shown in Fig. 3(a). The low-pressure spectrum has two peaks around 120 cm^{-1} (E_g) and 190 cm^{-1} (A_{1g}), respectively [58], in agreement to previous results [59]. The two peaks shift to higher frequency as the pressure increases. Above 17 GPa, two new peaks appear, indicating the lowering of crystalline symmetry, consistent with our XRD results.

In Figure 3(b), we compare the frequencies of the calculated and observed Raman-active modes [60]. The pressure dependence of the high-energy E-type mode is in excellent agreement with the experimental results, clearly showing the structural phase transition in the 17–20 GPa range. The high-energy A-type mode, while it is appreciably underestimated compared to experiment, does exhibit a similar trend, as discussed in the Supplemental Material [24]. After the phase transition, the in-plane unit cell triples in size and two additional Raman-active modes appear, consistent with the Raman measurements. The low-energy A-type mode in the $H2$ phases hardens with increasing pressure, and follows closely the experimental data [61]. The medium-energy E-type mode (~ 100 cm^{-1}) is slightly downshifted compared to experiment, but displays a similar pressure dependence [62].

A comparison between the electronic structures of the $H1$ and $H2$ compounds reveals that the phase transition leads to significant changes. In particular, we find avoided crossings near the Fermi level along Γ-M', Γ-K', and Γ-A
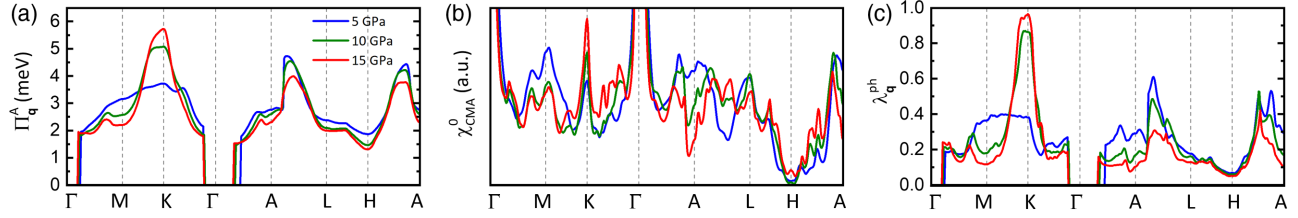
FIG. 4.   (a) The FS contribution to the adiabatic phonon self-energy, (b) the static bare susceptibility in the constant matrix approximation, and (c) the EPC strength for the soft phonon mode in the three-atom $H1$ structure at various pressures [72]. These results provide evidence that both FS nesting and electron-phonon interactions play crucial parts in the observed phase transition of SnSe$_2$.

directions in the $H2$ phases (Supplemental Figs. S6 and S7 [24]). These changes are due to structural displacements originating from a phonon mode (Supplemental Fig. S13 [24]), pointing towards a sizable EPC of that phonon with electronic states near the Fermi level [63,64]. The deformation of the band structure is accompanied by a suppression of large parts of the FS (Supplemental Fig. S14 [24]), and an increasing removal of electronic weight at the Fermi level with increasing pressure (Supplemental Fig. S10(d) [24]). Similar characteristics have been observed in previous theoretical studies of CDW order in metallic TMDs [10,11,44,45].

Usually, the appearance of a superlattice is the signature of a CDW transition in low-dimensional systems giving rise to the question of whether the transitions are driven primarily by an instability of the electronic subsystem, the vibrational subsystem, or both. In metallic TMDs it has been shown that the wave vector dependence of the EPC drives the CDW formation, while the FS nesting has been found to play a minor role [9–11,44,45]. In particular, the breaking of electronic degeneracies by a phonon-modulated lattice distortion, the reduction of the density of states at the Fermi level, and the softening of a low-energy phonon are key signatures of a momentum-dependent electron-phonon coupling CDW instability.

To understand the phonon softening with pressure and to investigate the mechanisms behind the phase transition, we calculated the FS contribution to the adiabatic phonon self-energy $\Pi^A_{\mathbf{q},\nu}$ [65] for the soft phonon mode of the three-atom $H1$ phase [66]. As shown in Fig. 4(a), $\Pi^A_{\mathbf{q},\nu}$ increases dramatically with pressure at the K point, explaining the observed phonon softening and instability towards a transition to the $H2$ phase. In order to separate the purely electronic effects from that of the electron-phonon interaction, we calculated the bare susceptibility χ^0_{CMA} in the constant matrix approximation [70] and the EPC strength $\lambda^{\text{ph}}_{\mathbf{q},\nu}$ [see Figs. 4(b) and 4(c)]. Both χ^0_{CMA} and $\lambda^{\text{ph}}_{\mathbf{q},\nu}$ show a strong increase at the K point with increasing pressure, indicating that both FS nesting and electron-phonon interactions play crucial parts in the observed phase transition of SnSe$_2$. We find that the largest contributions to the FS nesting come from aligning the Γ-centered surface with the K-centered one (Supplemental Fig. S14(a) [24]). This

observation is in contrast to findings in metallic TMDs, where FS nesting was found to play a less significant role in the transition, as mentioned above [10,11,45,71].

The application of pressure would usually suppress the CDW in metallic TMDs [3,5]. Our result shows an example of the opposite situation: the pressure can actually induce a PLD (and possibly CDW) in a semiconducting TMD-related material. Although pressure-induced metallization was also observed in many semiconducting TMDs, no evidence of pressure-induced PLD (or CDW) has been observed so far, according to our knowledge in TMD-related materials. We expect that future research will show if the PLD observed here is related to a true CDW quantum state [73].

In conclusion, we find a pressure-induced phase transition in SnSe$_2$, which we investigated in detail by means of XRD, Raman and transport measurements, as well as first-principles calculations. Our experiments and calculations are overall in very good agreement with each other. We have shown that following the phonon instability naturally leads to the transition to a supercell structure, whose electronic and vibrational properties match our experimental findings. We further provide evidence that the observed phase transition is due to the combined effect of strong FS nesting and EPC at a momentum wave vector $\mathbf{q} = (1/3, 1/3, 0)$. To our knowledge, the formation of a $(1/3, 1/3, 0)$-type superlattice with application of pressure was never observed in TMD-related materials. Our discovery of pressure-induced structural modulation, therefore, offers exciting new possibilities and provides a new playground to study PLD and possible CDW phases in TMD-related materials.

*rmargine@binghamton.edu

[1] Q. H. Wang, K. Kalantar-Zadeh, A. Kis, J. N. Coleman, and M. S. Strano, Nat. Nanotechnol. 7, 699 (2012).

[2] M. Chhowalla, H. S. Shin, G. Eda, L.-J. Li, K. P. Loh, and H. Zhang, Nat. Chem. 5, 263 (2013).

[3] B. Sipos, A. F. Kusmartseva, A. Akrap, H. Berger, L. Forró, and E. Tutiš, Nat. Mater. 7, 960 (2008).

[4] A. P. Nayak, S. Bhattacharyya, J. Zhu, J. Liu, X. Wu, T. Pandey, C. Jin, A. K. Singh, D. Akinwande, and J.-F. Lin, Nat. Commun. 5, 3731 (2014).

[5] A. F. Kusmartseva, B. Sipos, H. Berger, L. Forró, and E. Tutiš, Phys. Rev. Lett. 103, 236401 (2009).

[6] J. A. Wilson, F. J. Di Salvo, and S. Mahajan, Adv. Phys. 24, 117 (1975).

[7] F. J. Di Salvo, D. E. Moncton, and J. V. Waszczak, Phys. Rev. B 14, 4321 (1976).

[8] K. Rossnagel, J. Phys. Condens. Matter 23, 213001 (2011).

[9] M. D. Johannes and I. I. Mazin, Phys. Rev. B 77, 165135 (2008).

[10] M. Calandra and F. Mauri, Phys. Rev. Lett. 106, 196406 (2011).

[11] C. Heil, S. Poncé, H. Lambert, M. Schlipf, E. R. Margine, and F. Giustino, Phys. Rev. Lett. 119, 087003 (2017).

[12] M. N. Ali, J. Xiong, S. Flynn, J. Tao, Q. D. Gibson, L. M. Schoop, T. Liang, N. Haldolaarachchige, M. Hirschberger, N. P. Ong, and R. J. Cava, Nature (London) 514, 205 (2014).

[13] A. A. Soluyanov, D. Gresch, Z. Wang, Q. Wu, M. Troyer, X. Dai, and B. A. Bernevig, Nature (London) 527, 495 (2015).

[14] Y. Sun, S.-C. Wu, M. N. Ali, C. Felser, and B. Yan, Phys. Rev. B 92, 161107 (2015).

[15] Z.-H. Chi, X.-M. Zhao, H. Zhang, A. F. Goncharov, S. S. Lobanov, T. Kagayama, M. Sakata, and X.-J. Chen, Phys. Rev. Lett. 113, 036802 (2014).

[16] D. Kang, Y. Zhou, W. Yi, C. Yang, J. Guo, Y. Shi, S. Zhang, Z. Wang, C. Zhang, S. Jiang, A. Li, K. Yang, Q. Wu, G. Zhang, L. Sun, and Z. Zhao, Nat. Commun. 6, 7804 (2015).

[17] X.-C. Pan, X. Chen, H. Liu, Y. Feng, Z. Wei, Y. Zhou, Z. Chi, L. Pi, F. Yen, F. Song, X. Wan, Z. Yang, B. Wang, G. Wang, and Y. Zhang, Nat. Commun. 6, 7805 (2015).

[18] Y. Qi, P. G. Naumov, M. N. Ali, C. R. Rajamathi, W. Schnelle, O. Barkalov, M. Hanfland, S.-C. Wu, C. Shekhar, Y. Sun, V. Süß, M. Schmidt, U. Schwarz, E. Pippel, P. Werner, R. Hillebrand, T. Förster, E. Kampert, S. Parkin, R. J. Cava et al., Nat. Commun. 7, 11038 (2016).

[19] G. Domingo, R. S. Itoga, and C. R. Kannewurf, Phys. Rev. 143, 536 (1966).

[20] P. Yu, X. Yu, W. Lu, H. Lin, L. Sun, K. Du, F. Liu, W. Fu, Q. Zeng, Z. Shen, C. Jin, Q. J. Wang, and Z. Liu, Adv. Funct. Mater. 26, 137 (2016).

[21] R. Y. Wang, M. A. Caldwell, R. G. D. Jeyasingh, S. Aloni, R. M. Shelby, H.-S. P. Wong, and D. J. Milliron, J. Appl. Phys. 109, 113506 (2011).

[22] H. Yu, W. Lao, L. Wang, K. Li, and Y. Chen, Phys. Rev. Lett. 118, 137002 (2017).

[23] K. Nguyen-Cong, J. M. Gonzalez, B. A. Steele, and I. I. Oleynik, arXiv:1709.07570.

[24] See Supplemental Material at http://link.aps.org/supplemental/10.1103/PhysRevLett.121.027003 for further details on the experimental measurements and first-principles calculations, as well as Table S1, Figs. S(1)–S(14), and Refs. [25–38].

[25] http://www.hqgraphene.com.

[26] A. G. Gavriliuk, A. A. Mironovich, and V. V. Struzhkin, Rev. Sci. Instrum. 80, 043906 (2009).

[27] P. E. Blöchl, Phys. Rev. B 50, 17953 (1994).

[28] J. P. Perdew, K. Burke, and M. Ernzerhof, Phys. Rev. Lett. 77, 3865 (1996); 78, 1396 (1997).

[29] J. Klimeš, D. R. Bowler, and A. Michaelides, J. Phys. Condens. Matter 22, 022201 (2009); Phys. Rev. B 83, 195131 (2011).

[30] H. J. Monkhorst and J. D. Pack, Phys. Rev. B 13, 5188 (1976).

[31] A. Togo and I. Tanaka, Scr. Mater. 108, 1 (2015).

[32] M. Schlipf and F. Gygi, Comput. Phys. Commun. 196, 36 (2015).

[33] E. Kroumova, M. I. Aroyo, J. M. Perez-Mato, A. Kirov, C. Capillas, S. Ivantchev, and H. Wondratschek, Phase Transitions 76, 155 (2003).

[34] M. I. Aroyo, J. M. Perez-Mato, D. Orobengoa, E. Tasci, G. de la Flor, and A. Kirov, Bulg Chem Commun 43, 183 (2011).

[35] K. Lee, É. D. Murray, L. Kong, B. I. Lundqvist, and D. C. Langreth, Phys. Rev. B 82, 081101 (2010).

[36] S. Grimme, J. Comput. Chem. 27, 1787 (2006).

[37] D. M. Ceperley and B. J. Alder, Phys. Rev. Lett. 45, 566 (1980).

[38] J. P. Perdew and A. Zunger, Phys. Rev. B 23, 5048 (1981).

[39] G. Busch, C. Fröhlich, F. Hulliger, and E. Steigmeier, Helv. Phys. Acta 34, 359 (1961).

[40] We should note that the two imaginary modes are either degenerate or nearly degenerate in VASP [41,42] and QUANTUM ESPRESSO [43] calculations, respectively.

[41] G. Kresse and J. Furthmüller, Phys. Rev. B 54, 11169 (1996).

[42] G. Kresse and J. Hafner, Phys. Rev. B 47, 558 (1993).

[43] P. Giannozzi et al., J. Phys. Condens. Matter 21, 395502 (2009).

[44] M. Calandra, I. I. Mazin, and F. Mauri, Phys. Rev. B 80, 241108 (2009).

[45] F. Weber, S. Rosenkranz, J.-P. Castellan, R. Osborn, R. Hott, R. Heid, K.-P. Bohnen, T. Egami, A. H. Said, and D. Reznik, Phys. Rev. Lett. 107, 107403 (2011).

[46] A. N. Kolmogorov, S. Shah, E. R. Margine, A. K. Kleppe, and A. P. Jephcoat, Phys. Rev. Lett. 109, 075501 (2012).

[47] These displacements involve in-plane and out-of-plane movements of the Se and Sn atoms, respectively, as depicted in Supplemental Fig. S3 for the A_{2g} and A_{2u} phonons [24].

[48] Subsequent phonon calculations also revealed that all phonon branches for these $H2$ phases at the Γ point are

positive, indicating that the structures are dynamically stable at 30 GPa.

[49] The space groups were found with the ISOTROPY software [50] interfaced with the MAISE package [51] using a tolerance of 0.01.

[50] ISOTROPY Software Suite, http://www.iso.byu.edu.

[51] S. Hajinazar, J. Shao, and A. N. Kolmogorov, Phys. Rev. B **95**, 014114 (2017).

[52] T. Minagawa, J. Phys. Soc. Jpn. **49**, 2317 (1980).

[53] The slightly lower $H1$-to-$H2$ transition pressure in the transport measurements, i.e., 15 GPa compared to 17 GPa in the XRD and Raman experiments, originates from the different pressure media employed [24].

[54] We examined the effect of the spin-orbit coupling and found it to induce only minor changes in the electronic band structure in agreement with a previous study [55].

[55] J. M. Gonzalez and I. I. Oleynik, Phys. Rev. B **94**, 125443 (2016).

[56] P. Manou, J. A. Kalomiros, A. N. Anagnostopoulos, and K. Kambas, Mater. Res. Bull. **31**, 1407 (1996).

[57] A. Bera, A. Singh, D. V. S. Muthu, U. V. Waghmare, and A. K. Sood, J. Phys. Condens. Matter **29**, 105403 (2017).

[58] The two Raman-active modes originate from the in-plane (E_g) and out-of-plane (A_{1g}) displacements of Se atoms.

[59] A. J. Smith, P. E. Meek, and W. Y. Liang, J. Phys. C **10**, 1321 (1977).

[60] The corresponding two Raman-active modes in the $H2$ phases are referred to as E-type and A-type modes. A brief discussion on the irreducible representations of the optical zone-center phonons is given in the Supplemental Material [24].

[61] This mode involves only in-plane displacements of Se atoms and primarily out-of-plane displacements of Sn atoms.

[62] This mode involves only out-of-plane displacements of Se atoms and primarily in-plane displacements of Sn atoms.

[63] M. I. Katsnelson and A. V. Trefilov, JETP Lett. **42**, 485 (1985).

[64] M. I. Katsnelson, I. I. Naumov, and A. V. Trefilov, Phase Transit. **49**, 143 (1994).

[65] P. Zhang, S. G. Louie, and M. L. Cohen, Phys. Rev. Lett. **94**, 225502 (2005).

[66] The calculation of the electron-phonon interactions, bare susceptibilities and phonon self-energies were obtained with the EPW code [67,68] of the QUANTUM ESPRESSO distribution [43], in conjunction with the Wannier90 library [69]. Details about these calculations are given in the Supplemental Material [24].

[67] F. Giustino, M. L. Cohen, and S. G. Louie, Phys. Rev. B **76**, 165108 (2007).

[68] S. Poncé, E. R. Margine, C. Verdi, and F. Giustino, Comput. Phys. Commun. **209**, 116 (2016).

[69] A. A. Mostofi, J. R. Yates, G. Pizzi, Y.-S. Lee, I. Souza, D. Vanderbilt, and N. Marzari, Comput. Phys. Commun. **185**, 2309 (2014).

[70] C. Heil, H. Sormann, L. Boeri, M. Aichhorn, and W. von der Linden, Phys. Rev. B **90**, 115143 (2014).

[71] T. Valla, A. V. Fedorov, P. D. Johnson, P. A. Glans, C. McGuinness, K. E. Smith, E. Y. Andrei, and H. Berger, Phys. Rev. Lett. **92**, 086401 (2004).

[72] The FS contribution to the adiabatic phonon self-energy is

$$\Pi^A_{\mathbf{q},\nu} = \sum_{m,n} \int \frac{d\mathbf{k}}{\Omega_{\mathrm{BZ}}} |g_{mn,\nu}(\mathbf{k},\mathbf{q})|^2 \left[\frac{f_{n,\mathbf{k}} - f_{m,\mathbf{k+q}}}{\epsilon_{m,\mathbf{k+q}} - \epsilon_{n,\mathbf{k}}} \right]$$
$$\Theta(|\epsilon_{m,\mathbf{k+q}} - \epsilon_F| < \epsilon_c)\Theta(|\epsilon_{n,\mathbf{k}} - \epsilon_F| < \epsilon_c), \qquad (1)$$

with electron band indices m, n, phonon mode index ν, reciprocal wave vectors $\mathbf{k}$, $\mathbf{q}$, electron-phonon matrix element $g_{mn,\nu}$, Fermi distribution function f, Brillouin zone volume Ω_{BZ}, and Fermi energy ϵ_F. The step function Θ with an energy cutoff $\epsilon_c = 100$ meV ensures that only states close to the Fermi level are contributing to the self-energy, the qualitative results are insensitive to the choice of ϵ_c. To avoid numerical instabilities due to very small phonon energies for $\mathbf{q} \to 0$, the EPC around Γ for acoustic phonon frequencies smaller than 2.5 meV have been set to zero. The static bare susceptibility χ^0_{CMA} in the constant matrix approximation has been calculated by setting all electron-phonon matrix elements $g_{mn,\nu}$ in the expression of $\Pi^A_{\mathbf{q},\nu}$ to unity, in order to separate purely electronic effects coming from the denominator from electron-phonon interaction effects. The EPC strength associated with a specific phonon mode ν and wave vector $\mathbf{q}$ is

$$\lambda^{\mathrm{ph}}_{\mathbf{q},\nu} = \frac{1}{N(\epsilon_F)\omega_{\mathbf{q},\nu}} \sum_{m,n} \int \frac{d\mathbf{k}}{\Omega_{\mathrm{BZ}}} |g_{mn,\nu}(\mathbf{k},\mathbf{q})|^2$$
$$\times \delta(\epsilon_{m,\mathbf{k+q}} - \epsilon_F)\delta(\epsilon_{n,\mathbf{k}} - \epsilon_F), \qquad (2)$$

where $N(\epsilon_F)$ is the density of states per spin at the Fermi level.

[73] P. Monceau, Adv. Phys. **61**, 325 (2012).